

NRC Publications Archive Archives des publications du CNRC

In vivo brain delivery of BBB-enabled iduronate 2-sulfatase in rats

Costain, Will J.; Haqqani, Arsalan S.; Hussack, Greg; Van Faassen, Henk; Lessard, Etienne; Ling, Binbing; Brunette, Eric; Ly, Dao; Fang, Hung; Bultinck, Jennyfer; Geysens, Steven; Pynaert, Gwenda; Piens, Kathleen; Ryckaert, Stefan; Fudalej, Franck; Vervecken, Wouter; Stanimirovic, Danica

This publication could be one of several versions: author's original, accepted manuscript or the publisher's version. / La version de cette publication peut être l'une des suivantes : la version prépublication de l'auteur, la version acceptée du manuscrit ou la version de l'éditeur.

For the publisher's version, please access the DOI link below. / Pour consulter la version de l'éditeur, utilisez le lien DOI ci-dessous.

Publisher's version / Version de l'éditeur:

<https://doi.org/10.1186/s12987-024-00617-6>

Fluids and Barriers of the CNS, 22, 1, 2025-01-14

NRC Publications Archive Record / Notice des Archives des publications du CNRC :

<https://nrc-publications.canada.ca/eng/view/object/?id=756f5026-6d2b-4352-847b-016de5538d13>

<https://publications-cnrc.canada.ca/fra/voir/objet/?id=756f5026-6d2b-4352-847b-016de5538d13>

Access and use of this website and the material on it are subject to the Terms and Conditions set forth at

<https://nrc-publications.canada.ca/eng/copyright>

READ THESE TERMS AND CONDITIONS CAREFULLY BEFORE USING THIS WEBSITE.

L'accès à ce site Web et l'utilisation de son contenu sont assujettis aux conditions présentées dans le site

<https://publications-cnrc.canada.ca/fra/droits>

LISEZ CES CONDITIONS ATTENTIVEMENT AVANT D'UTILISER CE SITE WEB.

Questions? Contact the NRC Publications Archive team at

PublicationsArchive-ArchivesPublications@nrc-cnrc.gc.ca. If you wish to email the authors directly, please see the first page of the publication for their contact information.

Vous avez des questions? Nous pouvons vous aider. Pour communiquer directement avec un auteur, consultez la première page de la revue dans laquelle son article a été publié afin de trouver ses coordonnées. Si vous n'arrivez pas à les repérer, communiquez avec nous à PublicationsArchive-ArchivesPublications@nrc-cnrc.gc.ca.

RESEARCH

Open Access



In vivo brain delivery of BBB-enabled iduronate 2-sulfatase in rats

Will J. Costain^{1*}, Arsalan S. Haqqani¹, Greg Hussack¹, Henk van Faassen¹, Etienne Lessard¹, Binbing Ling¹, Eric Brunette¹, Dao Ly¹, Hung Fang¹, Jennyfer Bultinck², Steven Geysens², Gwenda Pynaert², Kathleen Piens², Stefan Ryckaert², Franck Fudalej², Wouter Verweken² and Danica Stanimirovic¹

Abstract

Background Iduronate-2-sulfatase (IDS) deficiency (MPS II; Hunter syndrome) is a disorder that exhibits peripheral and CNS pathology. The blood brain barrier (BBB) prevents systemic enzyme replacement therapy (ERT) from alleviating CNS pathology. We aimed to enable brain delivery of systemic ERT by using molecular BBB-Trojans targeting endothelial transcytosis receptors. Methods: Single-domain antibody (sdAb)-enzyme fusion protein constructs were prepared in *Yarrowia lipolytica*. sdAb affinity and BBB permeability were characterized using SPR and an in vitro rodent BBB assay, respectively. In vivo pharmacokinetic (PK) analysis was performed in rats. Quantification of fusion protein amounts were performed using LC-MS.

Results Fusion proteins consisting of IDS and BBB-transmigrating sdAbs, albumin binding sdAbs or human serum albumin (HSA) were evaluated for their in vitro BBB permeability. IGF1R3H5-IDS was selected for in vivo PK analysis in rats. IDS and IGF1R3H5-IDS exhibited very short (< 10 min) serum half-life ($t_{1/2\alpha}$), while constructs containing either HSA or anti-serum albumin sdAbs (R28 or M79) showed 8–11 fold increases in the area under the curve (AUC) in serum. CSF analysis indicated that IGF1R3H5 increased brain exposure by 9 fold (AUC) and constructs containing HSA or R28 exhibited 42–52 fold increases. Quantitation of brain levels confirmed the increased and sustained delivery of IDS to the brain of HSA- and R28-containing constructs. Lastly, analysis of brain fractions demonstrated that the increases in brain tissue were due to parenchymal delivery without fusion protein accumulation in brain vessels.

Conclusions These results demonstrate the utility of IGF1R-targeting sdAbs to effect brain delivery of lysosomal enzymes, as well as the utility of serum albumin-targeting sdAbs in $t_{1/2}$ extension, to increase brain delivery of rapidly cleared enzymes.

Keywords Blood brain barrier, MPS II, Iduronate-2-sulfatase, Enzyme replacement therapy, CSF, Brain, Pharmacokinetics

*Correspondence:

Will J. Costain

Will.Costain@nrc-cnrc.gc.ca

¹Human Health Therapeutics Research Centre, National Research Council
Canada, Ottawa, ON, Canada

²Oxyrane, Ghent, Belgium



© Crown 2024. **Open Access** This article is licensed under a Creative Commons Attribution 4.0 International License, which permits use, sharing, adaptation, distribution and reproduction in any medium or format, as long as you give appropriate credit to the original author(s) and the source, provide a link to the Creative Commons licence, and indicate if changes were made. The images or other third party material in this article are included in the article's Creative Commons licence, unless indicated otherwise in a credit line to the material. If material is not included in the article's Creative Commons licence and your intended use is not permitted by statutory regulation or exceeds the permitted use, you will need to obtain permission directly from the copyright holder. To view a copy of this licence, visit <http://creativecommons.org/licenses/by/4.0/>.

Background

Lysosomal storage diseases (LSDs) are a group of approximately 50 rare inherited metabolic disorders that result from defects in lysosomal function. LSDs are typically the consequence of a deficiency of a single enzyme required for the metabolism of lipids, glycoproteins and mucopolysaccharides. The disease is caused by excessive accumulation of non-processed material (such as heparan sulfate and dermatan sulfate) in cells and tissues, resulting in gross abnormalities in development and mental retardation when the central nervous system (CNS) is affected [1]. At least 75% of all LSDs have a significant CNS pathology [2]. The current standard of care for LSDs is enzyme replacement therapy (ERT), consisting of the intravenous administration of a recombinant form of the affected enzyme. Although ERT has been successful in treating peripheral symptoms by improving enzyme activity in peripheral organs such as liver, kidneys, spleen and heart, it is ineffective in the treatment of CNS pathologies because of the inability of peripherally-administered enzymes to cross the blood-brain barrier (BBB) and consequently reach the CNS [3, 4].

The BBB is formed by specialized endothelial cells of brain microvessels and capillaries joined together by tight junctions that restrict paracellular transport of hydrophilic molecules >500 Da. Polarized efflux transporters, also present in the BBB, further prevent brain access to many lipophilic synthetic molecules [5]. Systemic delivery of large complex therapeutics, such as enzymes and nanoparticles, across the BBB was not considered feasible until the recent development of novel delivery technologies focused on trans-cellular pathways that harness receptor-mediated transcytosis (RMT) mechanisms [6]. Recent demonstrations of enzyme delivery to the CNS using antibodies targeting the transferrin receptor (TfR) have been reported [7, 8]. However, TfR lacks brain-specific expression and safety concerns emerged during pre-clinical evaluations of TfR antibodies stemming from TfR enrichment in reticulocytes, lungs and neurons [6].

Here, we used single-domain antibodies (sdAbs, VHHs) capable of transigrating the BBB by RMT (referred to as 'BBB Trojans') [9–11], to functionalize CNS delivery of iduronate-2-sulfatase (IDS), an enzyme deficient in patients with mucopolysaccharidosis type II (MPS II; Hunter syndrome). We have previously developed multiple sdAbs capable of BBB transcytosis, with the 1st-generation BBB Trojan FC5 binding transmembrane protein 30 A (TMEM30A [12]), and 2nd-generation BBB Trojans binding insulin-like growth factor 1 receptor (IGF1R [13]). In this work we demonstrate that BBB Trojans, when fused to IDS, enabled BBB transmigration in a rat in vitro BBB model and in rodents. We found a major limitation to CNS delivery was the exceptionally short serum half-life ($t_{1/2}$) of IDS. We addressed this by

extending serum $t_{1/2}$ through fusion to either human serum albumin (HSA), or sdAbs that bind serum albumin [14, 15]. Our dual functionalization strategy resulted in dramatic increases in CNS delivery (cerebrospinal fluid and brain) of IDS. Lastly, we used brain fractionation to demonstrate that CNS-enabled IDS was successfully delivered to the brain parenchyma.

Materials and methods

Protein design and production

Various recombinant proteins (Supplemental Fig. 1) comprised of IDS alone, or as fusions to sdAbs and/or HSA were designed, expressed and purified. A *Yarrowia lipolytica* yeast strain OXY5632, co-expressing *Bos taurus* formylglycine generating enzyme [54], was created to produce catalytically active IDS constructs. This strain is glyco-engineered to obtain glycoproteins with high levels of phosphorylated N-glycans [55, 56]. The fermentation and subsequent harvest steps were performed as described previously [55], after which the clarified medium containing the target protein (such as IGF1R3H5-IDS) was subjected to multiple chromatography steps to yield the pure product. The purification protocol consisted of a Ni-immobilized metal-affinity chromatography (IMAC) capturing step to remove the majority of the contaminants, followed by an enzymatic treatment with Jack bean α -mannosidase (JMan) at pH 4.5 to uncap the shielded mannose-6-phosphate (Man-6-P) and further trim terminal α -linked mannose residues from the protein-linked N-glycans. A second Ni-IMAC step was used to remove JMan. The final samples were formulated by diafiltration in 20 mM sodium phosphate, 137 mM NaCl, pH 6.2. The same production and purification method was used for all recombinant proteins described in this study. In one case, the IGF1R3H5-IDS-HSA(K573P) construct, hereafter referred to as IGF1R3H5-IDS-HSA, required an extra polishing step to reach the same level of purity as the other constructs.

Surface plasmon resonance (SPR)

SPR was used to determine the affinities of sdAbs (anti-IGF1R or anti-serum albumin) and IDS fusion constructs for their respective targets, essentially as previously described [15, 41]. SPR analysis was performed at 25 °C on a Biacore T200 or a Biacore 3000 (Cytiva, Vancouver, Canada) using HBS-EP running buffer (10 mM HEPES, pH 7.4, containing 150 mM NaCl, 3 mM EDTA and 0.005% v/v surfactant P20 (polyoxyethylene 20 sorbitan monolaurate); Cytiva), or HBS-EP + running buffer (10 mM HEPES, 150 mM NaCl, 3 mM EDTA, pH 7.4, 0.05% P20; Cytiva), respectively. Human IGF1R (391-GR-050, R&D Systems, Minneapolis, MN) and rhesus IGF1R [41] were immobilized on a CM4 chip at high density (~2,500 RUs) in 10 mM acetate buffer, pH 4.0. Variable

concentrations of the analytes (sdAbs, IDS fusions) were flowed at 40 $\mu\text{L}/\text{min}$, with contact and dissociations times of 300 and 400 s, respectively. The surface was regenerated in 10 mM glycine, pH 5.5. Similarly, HSA (A3782, MilliporeSigma, Oakville, Canada) or rat serum albumin (RSA, A6414, MilliporeSigma) were immobilized on CM4 sensorchips (~1500 RUs of HSA and RSA) in 10 mM acetate buffer, pH 4.5. Variable concentrations of analytes were flowed at 40 $\mu\text{L}/\text{min}$, with contact and dissociations times of 300 and 400 s, respectively. The surface was regenerated in 10 mM glycine, pH 5.5. Reference flow cell subtracted sensorgrams were fit to a 1:1 binding model using BIAevaluation Software v3.2 (Biacore T200) or v4.1 (Biacore 3000).

In vitro BBB transcytosis model and permeability studies in SV-ARBEc cells

SV-ARBEcs were seeded at 80,000 cells/membrane on rat-tail collagen-coated 0.83 cm^2 Falcon cell inserts, 1 μm pore size, in 1 mL SV-ARBEc feeding medium without phenol red. The model characterization is described in detail in Garberg et al. [57]. For cell growth and maintenance prior to the assays, the wells of a 12-well tissue culture plate (i.e., bottom chamber) contained 2 mL of 50:50 (v/v) mixtures of SV-ARBEc medium without phenol red and rat astrocyte-conditioned medium. Pe[sucrose] was determined on inserts dedicated to

quality control (QC) assessment for each plating. Transport assays were conducted using the model when Pe[sucrose] was $<0.6 (\times 10^{-3}) \text{ cm}/\text{min}$. The Pe[sucrose] for the QC inserts from the experiments presented in Fig. 1 were $0.40 \pm 0.18 \times 10^{-3} \text{ cm}/\text{min}$. Transport experiments were performed exactly as described in Haqqani et al. [58] by adding a mixture of the test constructs in equimolar concentrations (2.5 μM) to the top chamber and by collecting 100 μL aliquots (with subsequent replacement with 100 μL of transport buffer) from the bottom chamber at 90 min for simultaneous quantification of all test constructs using the multiplexed selected reaction monitoring (SRM) method. The samples were diluted in transport buffer (TB; 5 mM MgCl_2 , 10 mM HEPES in Hanks' balanced salt solution (HBSS), pH 7.4) and added (1:1) to the top chamber containing SV-ARBEc media with 5% fetal bovine serum (FBS). For assays where samples were assessed by SRM, the bottom chamber contained TB. For each test construct, negative and positive control constructs were included in the transwell assay. All antibodies were present at the same concentration (2.5 M) in the top well. The A20.1 single domain antibody does not bind to a target on the SV-ARBEc cell surface and does not undergo RMT. A20.1-VHH was present in all inserts along with individual test constructs, was used as a negative control for RMT, and served as an additional QC for barrier integrity. Positive control antibodies (FC5-VHH, IGF1R5-VHH, IGF1R3H5-VHH) were also assessed with A20.1-VHH present in the same transwell inserts. The apparent permeability coefficient P_{APP} was calculated as described previously [59].

Biodistribution: CSF and brain collection

All animals were purchased from Charles River Laboratories International, Inc. (Wilmington, MA, USA). Animals were housed in groups of three in a 12 h light-dark cycle at a temperature of 24 $^\circ\text{C}$, a relative humidity of $50 \pm 5\%$, and were allowed free access to food and water. All animal procedures were approved by the NRC's Animal Care Committee and were in compliance with the Canadian Council of Animal Care guidelines. Female Wistar rats aged 8–10 wk (weight range, 135–185 g) were used for sample collection. Cerebrospinal fluid (CSF) and brain were collected to assess the biodistribution of the test articles. The animals were provided analgesia (sustained-release buprenorphine, 1.2 mg/kg) before the first CSF collection, as described previously [58, 60]. CSF was collected and analyzed according to the procedures described in Haqqani et al. [58]. Following CSF collection, the wound was then closed and a blood sample was collected from the tail vein, according to Flutterm et al. [61]. The rat was then returned to its home cage and housed in the recovery room until the next CSF collection. For subsequent CSF and blood collections, the rat

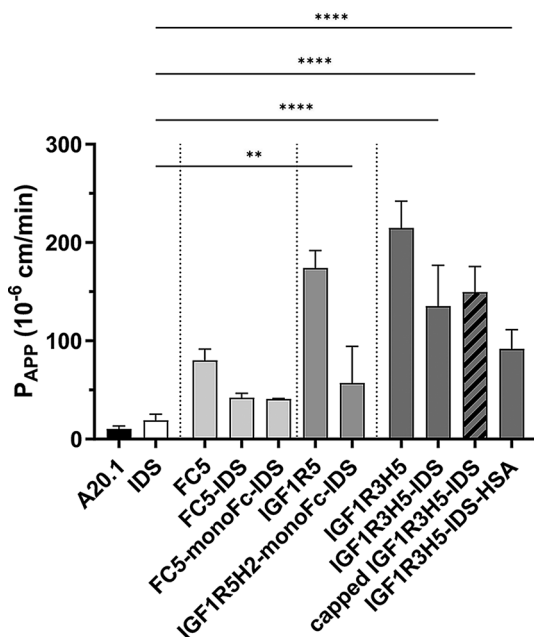


Fig. 1 BBB-Trojans enable permeability of IDS in a rat in vitro BBB model. IDS exhibits limited BBB permeability comparable to the negative control A20.1 VHH. Fusions of IDS with BBB-Trojans (FC5, IGF1R5H2 or IGF1R3H5) provide significantly greater BBB permeability relative to IDS and A20.1 VHH. Data are presented as mean \pm SD; one-way ANOVA with Šidák's multiple comparisons test (only significant differences between IDS and IDS fusions are shown), ** $P < 0.01$, **** $P < 0.0001$

was anaesthetized and the sutures removed. The muscles covering the cisterna magna were gently separated and the dura mater exposed. CSF sampling was then performed as described above. Approximately 15–20 μL of CSF can be collected at each time point. For the terminal CSF collection, approximately 50–100 μL of CSF can be collected and blood is collected by heart puncture. Finally, euthanasia is performed by cervical dislocation under deep isoflurane anesthesia.

Following collection of the last CSF sample, rats were sacrificed by cardiac puncture and the brains perfused with 20 mL saline supplemented with 1 EU/mL heparin (Organon, Toronto, Canada) at 2 mL/min and harvested. Brains were sectioned along the midline and the right hemisphere was frozen ($-80\text{ }^{\circ}\text{C}$) and stored for MRM processing.

Brain homogenization and processing

Prior to MRM analysis the entire right hemisphere was weighed while frozen and the middle third extracted and weighed (typically $\sim 0.16\text{ g}$). The remaining tissue was stored at $-80\text{ }^{\circ}\text{C}$. The brain tissue was then homogenized in 1 mL of ice-cold homogenization buffer (50 mM Tris-HCl, pH 8, 150 mM NaCl, 1.0% sodium deoxycholate (D6750, MilliporeSigma), and 1 \times protease inhibitor cocktail (P8340, MilliporeSigma)) using a Wheaton Dounce homogenizer (10–12 strokes with a Glas-Col drill (model# 099 C K54) at 60% speed, at $4\text{ }^{\circ}\text{C}$) until pieces of tissue were no longer detectable. Samples were sonicated (Fisher, Model 300 Sonic Dismembrator) on ice with three 10 s bursts at 30%, and insoluble material was removed by centrifugation ($20,000 \times g$ for 10 min at $4\text{ }^{\circ}\text{C}$). The supernatants were then transferred to new tubes on ice. Protein concentrations were then determined using the Bradford method with a standard curve based on bovine serum albumin (BSA Quick Start Standard; BioRad, cat# 500–0207). A 5 μL aliquot of the brain extract was diluted 1:5 in 25 mM ammonium bicarbonate (ABC; Sigma, cat# A6141), and a volume corresponding to 20 μg was transferred to a new tube. The 20 μg aliquot was made up to 12.5 μL with 25 mM ABC and 12.5 μL of 10% sodium deoxycholate (DOC; Sigma, cat# D6750) was added to give a concentration of 5% DOC. The samples were then vortexed and briefly centrifuged prior to the addition of 2.5 μL freshly prepared 10 \times DL-dithiothreitol (DTT; D9163, MilliporeSigma) to provide a concentration of 5 mM DTT. The samples were vortexed and centrifuged briefly and then incubated at $95\text{ }^{\circ}\text{C}$ for 10 min. The samples were then cooled, and briefly centrifuged prior to the addition of 2.75 μL 10 \times iodoacetamide (I1149, MilliporeSigma) to provide a concentration of 10 mM. The samples were vortexed and centrifuged prior to incubation at room temperature for 30 min in the dark. The samples were then diluted to 125.0 μL with 25 mM

ABC. A 2 μL (1 μg) aliquot of trypsin (Promega, cat# V511C) was then added to each sample, which were then mixed gently and briefly centrifuged prior to incubation in a Multitherm Incubator/Chiller unit (model H5000) at $37\text{ }^{\circ}\text{C}$ for 12 h and at $4\text{ }^{\circ}\text{C}$ thereafter. The samples were then stored at $-80\text{ }^{\circ}\text{C}$ until MRM analysis was conducted. Prior to MRM analysis, the DOC was precipitated by adding 15 μL AAF buffer (54% acetic acid, 150 mM ammonium acetate, 10% formic acid) to a 115 μL aliquot of the digested sample. The samples were then centrifuged at $50,400 \times g$ for 10 min at $4\text{ }^{\circ}\text{C}$, and 60 μL of the supernatant was transferred to a fresh vial. MRM analysis was performed using 20 μL of the supernatant.

In selected animals, brain homogenates of the left hemisphere were subjected to a vessel depletion protocol to obtain brain parenchyma and brain vessel fractions. The tissues were homogenized as above and sequential filtration through 100 μm and 20 μm nylon Nitex mesh filters (pluriSelect, Leipzig, Germany) was performed to obtain the brain fractions. To verify the efficacy of the vessel depletion procedure, the relative concentrations of markers of parenchyma (glial fibrillary acidic protein, GFAP) and vessels (platelet endothelial cell adhesion molecule, PECAM1) were determined in each sample prior to quantitation of the test articles using SRM as above (Suppl. Figure 2).

Serum pharmacokinetics analysis

At several post-injection timepoints, blood was collected and serum prepared to determine the serum half-life of the various constructs. Blood samples were taken from the lateral tail vein according to Fluttert et al. [61]. Samples were centrifuged (15 min at $21,100 \times g$; room temperature) and serum was stored at $-80\text{ }^{\circ}\text{C}$ until analysis. Serum and CSF concentration-time profiles were analyzed using WinNonlin software (Version 8.2, Pharsight Corporation, Mountain View, CA, USA).

Compartmental serum pharmacokinetic analysis

Serum concentration-time data were analyzed using naïve pooled and a two-compartment model with intravenous (i.v.) bolus input, first-order elimination, and macro-rate constants to estimate the following pharmacokinetic parameters: volume of distribution of the central compartment (V_1) and of the peripheral compartment (V_2), clearance (CL), inter-compartmental clearance (CL_D), overall elimination half-life ($t_{1/2\beta}$) and predicted area under the plasma concentration time curve from time 0 to infinity (AUC). Overall, goodness of fit was based upon the predicted estimate and percent coefficient of variation (% CV) for primary and secondary parameters, as well as inspection of residual plots between observed and predicted concentration-time data.

Non-compartmental CSF/serum pharmacokinetic analysis

Mean serum and CSF concentration values were used to generate a composite pharmacokinetic profile. A non-compartmental approach consistent with the i.v. route of administration and using the linear/log trapezoidal method was employed to estimate the area under the curve (AUC) of the serum concentration versus time and CSF concentration versus time. For both serum and CSF, the area under concentration versus time curve from the start of dose administration to the last observed quantifiable (AUC_{last}) was estimated. Estimation of average concentration ratios for AUC_{last} is reported as $(AUC_{CSF}/AUC_{Serum}) \times 100$.

nanoLC/MS/MS

The protein levels of the test constructs in ex vivo samples (serum, CSF and brain) were quantified using targeted nanoflow liquid chromatography tandem mass spectrometry (nanoLC MS/MS). Purified sdAbs, fusion proteins, and body fluid samples containing these proteins were reduced, alkylated, and trypsin digested using previously described protocols [58, 62]. Each protein was first analyzed by nanoLC-MS/MS (nanoAcquity UPLC (Waters, Milford, MA, USA) coupled to LTQ XL ETD MS (ThermoFisher, Waltham, MA, USA)) using data-dependent acquisition to identify all ionizable peptides,

and the 3–5 of the most intense fragment ions are chosen. An initial SRM assay was developed to monitor these fragments at attomole amounts of the digest. Fragments showing reproducible intensity ratios at low amounts (~ 100 – 300 amol; Pearson $r^2 \geq 0.95$) were considered stable and are chosen for the final SRM assay. The locations and identities of the peptides chosen for SRM are shown in Supplemental Fig. 1 and Supplemental Table 1. The blood contamination of CSF samples was evaluated by in-reaction monitoring of rat serum albumin levels using a nanoLC-SRM method as described previously [58]. Measurement of CSF protein concentration was used as a rapid quantitative and nonspecific method for identifying serum contaminated samples. Typical protein concentration of CSF is 0.2–0.4 mg/mL in rat. Protein concentrations >0.4 mg/mL were considered to be likely contaminated with blood. The serum albumin blood-CSF ratio was determined by multiple SRM analysis of CSF of the corresponding serum sample. Ratios less than 1500-fold were considered contaminated with blood and are excluded from further analyses.

Results

Characterization of sdAb-IDS fusion proteins

Recombinant IDS and various fusion proteins containing IDS (Supplemental Fig. 1), harboring high levels of phosphorylated glycans, were produced in the glyco-engineered *Y. lipolytica* strain (OXY5632). The size and identity of the proteins were characterized by SDS-PAGE and western blotting, as well as N-glycan analysis to verify site occupancy and mannose 6-phosphorylation (data not shown). The activity of the IDS domain was determined for all constructs, with specific IDS activity ranging from 15,000 to 30,000 U/mg (data not shown).

Functionality of the monomeric anti-IGF1R and anti-serum albumin sdAbs and various IDS fusion proteins were evaluated by SPR. Table 1 shows that IGF1R3H5, a humanized version of the IGF1R3 VHH, exhibited high affinity ($K_D = 7.5$ nM) to human IGF1R. In comparison, the IGFR3H5-IDS construct exhibited ≈ 6 -fold increase in K_D (40–46 nM) for human IGF1R. IDS alone did not bind human IGF1R as expected. The affinity of the IGF1R3H5 domain in the IGF1R3H5-IDS constructs to human IGF1R was not affected by the uncapping process, where the terminal Man-6-P moieties are exposed. The affinity of the IGFR3H5-IDS-HSA (144.7 kDa) construct was $K_D = 77$ nM and 84 nM for human and rhesus IGF1R, respectively, and was only slightly weaker than the IGF1R3H5-IDS (78.7 kDa) construct. The reduced affinity of the fusion proteins relative to the monomeric IGF1R VHH may be related to being in an N-terminus fusion configuration. Thus, the IGF1R3H5 fusion construct retains its ability to bind to the target IGF1R.

Table 1 SPR-derived kinetics and affinities of VHHs and IDS fusion constructs

Construct	Man6P	Target	k_a (1/Ms)	k_d (1/s)	K_D (M)
IGF1R3H5		h-IGF1R	3.34E+05	2.51E-03	7.51E-09
IDS		h-IGF1R	n.b.	n.b.	n.b.
IDS		r-IGF1R	n.b.	n.b.	n.b.
IGF1R3H5-IDS	-	h-IGF1R	7.19E+04	2.89E-03	4.02E-08
IGF1R3H5-IDS	+	h-IGF1R	6.40E+04	2.95E-03	4.61E-08
IGF1R3H5-IDS		r-IGF1R	n.d.	n.d.	n.d.
IGF1R3H5-IDS-HSA	+	h-IGF1R	3.96E+04	3.07E-03	7.73E-08
IGF1R3H5-IDS-HSA	+	rh-IGF1R	4.58E+04	3.86E-03	8.44E-08
M79		HSA	4.52E+06	0.126	2.78E-08 [#]
M79		RSA	1.56E+07	6.61E-02	1.58E-09 [#]
M79		h-IGF1R	n.b.	n.b.	n.b.
R28		HSA	1.14E+06	1.33E-02	1.17E-08 [#]
R28		RSA	2.29E+06	1.65E-03	7.21E-10 [#]
R28		h-IGF1R	n.b.	n.b.	n.b.
IGF1R3H5-IDS-M79		HSA	1.37E+05	0.265	1.94E-06
IGF1R3H5-IDS-M79		RSA	1.30E+05	4.36E-02	3.36E-07
IGF1R3H5-IDS-M79		h-IGF1R	n.d.	n.d.	n.d.
IGF1R3H5-IDS-R28		HSA	2.76E+04	3.29E-02	1.19E-06
IGF1R3H5-IDS-R28		RSA	1.71E+04	1.51E-03	8.81E-08
IGF1R3H5-IDS-R28		h-IGF1R	n.d.	n.d.	n.d.

IGF1R3H5, humanized VHH targeting insulin like growth factor 1 receptor (IGF1R); IDS, iduronate-2-sulfatase; HSA, human serum albumin (K573P); RSA, rat serum albumin; M79, VHH targeting serum albumin; R28, VHH targeting serum albumin; Man6P, mannose-6-phosphate; h-IGF1R, human IGF1R; r-IGF1R, rhesus IGF1R; n.b., no binding; n.d., not determined

[#] Determined in van Faassen et al. 2020 [15]

The monomeric anti-serum albumin sdAbs [15] showed low nM affinity toward human and rat serum albumins (Table 1). Similar to the anti-IGF1R sdAbs, the anti-serum albumin sdAbs (R28 and M79) exhibited reduced affinity as C-terminus fusion proteins in the IGF1R3H5-IDS-M79 and IGF1R3H5-IDS-R28 constructs, with $K_{DS} = 1.9 \mu\text{M}$ and $1.2 \mu\text{M}$ for HSA, and $K_{DS} = 336 \text{ nM}$ and 88 nM for RSA, respectively.

In vitro analysis of BBB permeability using a rat brain endothelial cell model

An in vitro rat BBB assay was performed to validate the ability of BBB Trojans FC5 [10, 16] and anti-IGF1R sdAbs [11, 17] to enable BBB permeability of IDS, and to identify a lead candidate for subsequent in vivo evaluation. As previously shown, the sdAb FC5 VHH exhibited significantly greater apparent permeability (P_{APP}) in the in vitro BBB assay than the non-crossing negative control sdAb A20.1 (a VHH that targets a bacterial toxin and is used here as a negative control for BBB crossing) (Fig. 1) [18]. Furthermore, the permeability of IDS was not statistically different from A20.1, thereby confirming that the enzyme had very low BBB permeability. The fusion constructs comprised of FC5 and IDS exhibited permeability that was significantly greater than A20.1, but substantially reduced in comparison to FC5-VHH and not significantly different from IDS (Fig. 1).

IGF1R-mediated RMT was evaluated using two distinct sdAbs. The P_{APP} of the parental VHHs (IGF1R3 and IGF1R5) was confirmed to be consistent with historical values (IGF1R5, ~ 200 ; IGF1R3, ~ 250) [11, 19]. A construct comprised of a humanized version of IGF1R5 VHH

(IGF1R5H2), monomeric Fc [20], and IDS (IGF1R5H2-monoFc-IDS) also exhibited significantly greater P_{APP} than IDS in the rat BBB assay (Fig. 1). While the P_{APP} of IGF1R5H2-monoFc-IDS was similar to that of FC5, the observed P_{APP} was substantially reduced (33%) in comparison to IGF1R5. A third BBB Trojan (IGF1R3H5, a humanized version of the IGF1R3 VHH) was evaluated and it was found that the P_{APP} of the IGF1R3H5-IDS construct was comparable (66%) to the positive control IGF1R3 (parental llama VHH) and far exceeded that of IDS and A20.1 (9% and 5%, respectively) (Fig. 1). Notably, the P_{APP} of a construct containing HSA(K573P) was comparable to that of IGF1R3H5-IDS (65%). Figure 1 also shows that the permeability of a construct lacking a terminal Man-6-P (capped IGF1R3H5-IDS) was not different from a version with terminal Man-6-P moieties on its glycans. Lastly, the P_{APP} of the IGF1R3H5-based fusion proteins (~ 150) was superior to the FC5 and IGF1R5H2 constructs, was sufficient to justify evaluation in an in vivo transport assay, and therefore selected for subsequent studies.

In vivo analysis of serum and CSF pharmacokinetics

The constructs IGF1R3H5-IDS and IGF1R3H5-IDS-HSA were selected for in vivo characterization. Two additional constructs comprised of IGF1R3H5-IDS fused to anti-serum albumin sdAbs (R28 and M79) were also evaluated [14]. Figure 2 shows the concentrations of IDS, IGF1R3H5-IDS, IGF1R3H5-IDS-HSA, IGF1R3H5-IDS-R28 and IGF1R3H5-IDS-M79 in rat serum following single bolus i.v. injections of equimolar doses (76 nmol/kg). The data indicate that both IDS and IGF1R3H5-IDS are rapidly cleared from the serum with kinetics ($\alpha_{1/2}$ and $\beta t_{1/2}$) that are similar (Table 2), with IGF1R3H5-IDS unexpectedly exhibiting a 57% greater area under the curve (AUC) relative to IDS (Suppl. Figure 3). Similarly, analysis of serum IDS concentrations based on IDS enzymatic activity confirmed that IDS and IGF1R3H5-IDS are rapidly cleared from the serum (Suppl. Figure 4). In comparison, the IGF1R3H5-IDS-HSA construct exhibited a significantly reduced serum clearance (CL) rate (0.07 mL/min/kg) compared to IGF1R3H5-IDS (0.5 mL/min/kg) and IDS (0.7 mL/min/kg). Consequently, IGF1R3H5-IDS-HSA exhibited a much longer serum half-life ($\alpha_{1/2} = 27.8 \text{ min}$, $\beta t_{1/2} = 36.9 \text{ h}$) than IGF1R3H5-IDS and IDS. Correspondingly, the elimination of IGF1R3H5-IDS-HSA was ~ 7 - to 11 -fold (according to serum AUC values) slower than the constructs lacking HSA (Table 2). The constructs containing the IGF1R- and serum albumin-binding VHHs (IGF1R3H5-IDS-M79 and IGF1R3H5-IDS-R28) exhibited reduced serum clearance and increased serum $t_{1/2}$ values similar to the HSA-containing construct. Unexpectedly, the serum clearance of IGF1R3H5-IDS-M79 and IGF1R3H5-IDS-R28 were less

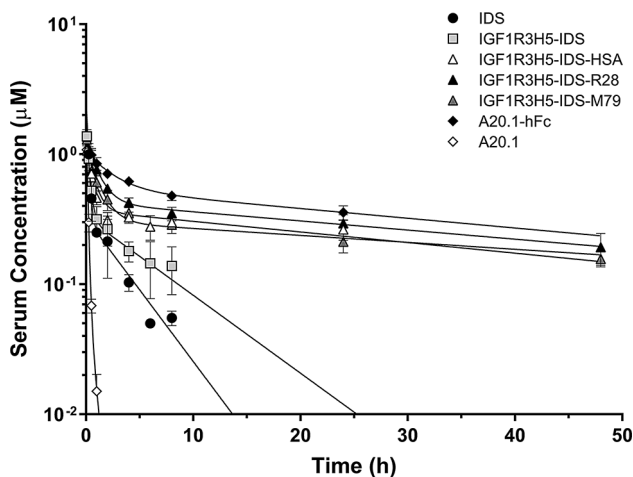


Fig. 2 Fusion of IDS with HSA or anti-serum albumin sdAbs (R28, M79) extends the serum half-life of IDS in rats. Serum concentrations of the constructs (observed versus predicted) were determined following i.v. administration at 76 nmol/kg. A20.1 VHH is rapidly eliminated and fusion with human Fc (hFc) dramatically reduced elimination from serum. IDS underwent rapid 2 phase elimination and fusion with HSA, R28 or M79 reduced elimination from serum. Values are shown as mean \pm SEM

Table 2 Mean PK parameter estimates (CV%) from 2-compartment analysis of serum concentration-time profiles after intravenous bolus administration of IDS constructs to Wistar rats ($n > 3$ per group, 76 nmol/kg)

Parameter	Units	IDS	IGF1R3H5-IDS	IGF1R3H5-IDS-HSA	IGF1R3H5-IDS-R28	IGF1R3H5-IDS-M79
C_{max}	nmol/mL	3 (45)	1.8 (8.8)	1.3 (3.3)	1.3 (3.9)	1.2 (6.2)
V	mL/kg	26.2 (45)	44.5 (8.8)	65.1 (3.3)	58.2 (3.9)	65.6 (6.2)
V_2	mL/kg	104 (13)	133 (12)	155 (11)	113 (6.2)	172 (11)
CL	mL/min/kg	0.7 (8.9)	0.5 (9.6)	0.07 (34)	0.05 (11)	0.05 (18)
CL ₂	mL/min/kg	1.4 (22)	1.8 (8)	1.1 (7.8)	0.6 (8.1)	0.7 (12)
AUC	nmol*min/mL	105 (8.9)	165 (9.6)	1212 (34)	1632 (11)	1540 (18)
$t_{1/2\alpha}$	Min	7.5 (29)	11.2 (12)	27.8 (10)	44.4 (11)	46.1 (15)
$t_{1/2\beta}$	Min	164 (10)	301 (17)	2216 (40)	2574 (14)	3383 (24)

C_{max} : Predicted peak concentration. $t_{1/2\alpha}$: Distribution half-life. $t_{1/2\beta}$: Elimination half-life. CL: total body clearance. CL₂: Intercompartmental clearance. V_1 : Central compartment volume of distribution. V_2 : Peripheral compartment volume of distribution. AUC: predicted area under the plasma concentration time curve from time 0 to infinity

than that observed for IGF1R3H5-IDS-HSA, which is reflected by the serum AUC values for IGF1R3H5-IDS-M79 and IGF1R3H5-IDS-R28 being 1.27- and 1.35-fold greater, respectively, than the AUC for IGF1R3H5-IDS-HSA. Thus, the anti-serum albumin containing constructs exhibited serum PK values that were consistent with the HSA containing construct, indicating that serum half-life extension was realized using two distinct strategies.

Analysis of test article levels in the CSF was conducted in order to evaluate the ability of IGF1R3H5 to effect BBB transcytosis in vivo. CSF PK is used to measure brain exposure to therapeutics and has been shown to correlate with delivery to brain parenchyma [9, 21]. Figure 3A compares protein concentrations of IDS, IGF1R3H5-IDS, IGF1R3H5-IDS-HSA and IGF1R3H5-IDS-R28 in rat CSF following single bolus i.v. injections of equimolar doses. The peak CSF concentrations of IGF1R3H5-IDS, IGF1R3H5-IDS-HSA and IGF1R3H5-IDS-R28 are similar, which is likely the result of the similar dosing levels employed. This is in stark contrast to the minimal amounts of IDS that were detected in CSF, thus confirming the capability of the IGF1R3H5 antibody to enable in vivo BBB transcytosis of IDS. Analyses of CSF levels of IGF1R3H5-IDS-HSA and IGF1R3H5-IDS-R28 indicate that maximum peak levels were observed 4 h post-administration, with detectable levels present 24 h post-administration (Fig. 3A). In comparison, peak CSF levels of IGF1R3H5-IDS were observed at 30–60 min post-administration and were virtually absent by 8 h post-administration. IGF1R3H5-IDS-HSA levels in CSF at 8 h post-administration were comparable to the peak levels observed for IGF1R3H5-IDS. Plotting the CSF / serum ratio shows that the peak levels in CSF represent ~0.5–0.6% of serum levels for the IGF1R3H5-containing constructs (Fig. 3B). Importantly, the IGF1R3H5-IDS-HSA and IGF1R3H5-IDS-R28 constructs exhibited distinctly prolonged CSF PK profiles, resulting in 49- and 61-fold increases, respectively, in the observed AUC compared to IDS (Table 3). Calculation of the AUC ratio (CSF /

serum) indicated that the IGR1R3H5-containing constructs exhibited a similar degree of brain exposure, with all constructs being improved by a factor of ~3–5 compared to IDS. These data emphasize the dramatic effect of serum half-life prolongation on increasing brain delivery. In contrast, the A20.1-hFc construct exhibited prolonged serum half-life with low CSF levels. As expected, the AUC ratio for A20.1-hFc was comparable to IDS (Table 3). Considering the unexpected serum PK extension observed with the inclusion of IGF1R3H5 (Tables 2 and 3), it appears that IGF1R3H5 and R28 act through an unpredicted mechanism to synergistically extend the serum PK of IDS.

In vivo analysis of brain levels.

Whole brain levels of IDS (1, 4 and 8 h), IGF1R3H5-IDS (1, 4, 8 and 24 h), IGF1R3H5-IDS-HSA (4 and 24 h only) and IGF1R3H5-IDS-R28 (4 and 24 h only) were quantified and Fig. 4 shows the test sample levels in rat brain over a 24-h period. Brain levels of IGF1R3H5-IDS were substantially greater than IDS at 1 and 4 h, with IDS no longer detected at 8 h. In comparison, detectable levels of IGF1R3H5-IDS-HSA and IGF1R3H5-IDS-R28 were observed in the brain at 4 and 24 h, indicating an increase in brain delivery that is commensurate with the observed CSF levels. This indicates that overall brain exposure was enhanced by the inclusion of HSA or R28. Figure 5 shows analyses of IDS, IGF1R3H5-IDS and IGF1R3H5-IDS-R28 in brain parenchyma and brain vessels. While IDS was detected in whole brain at 1 and 4 h post-administration (Fig. 4), IDS was below the detection limits in brain parenchyma and vessel samples from the same animals used for whole brain analyses (Fig. 5). In contrast, IGF1R3H5-IDS was detected in whole brain and brain parenchyma at 1 and 4 h. Moreover, IGF1R3H5-IDS was not detected in the brain vessel fraction, while IGF1R3H5-IDS-R28 was detected in whole brain as well as in brain parenchyma and vessels. Importantly, the IGF1R3H5-IDS and IGF1R3H5-IDS-R28 levels in brain parenchyma were much greater than in brain vessels. This indicates that retention of IGF1R3H5-containing

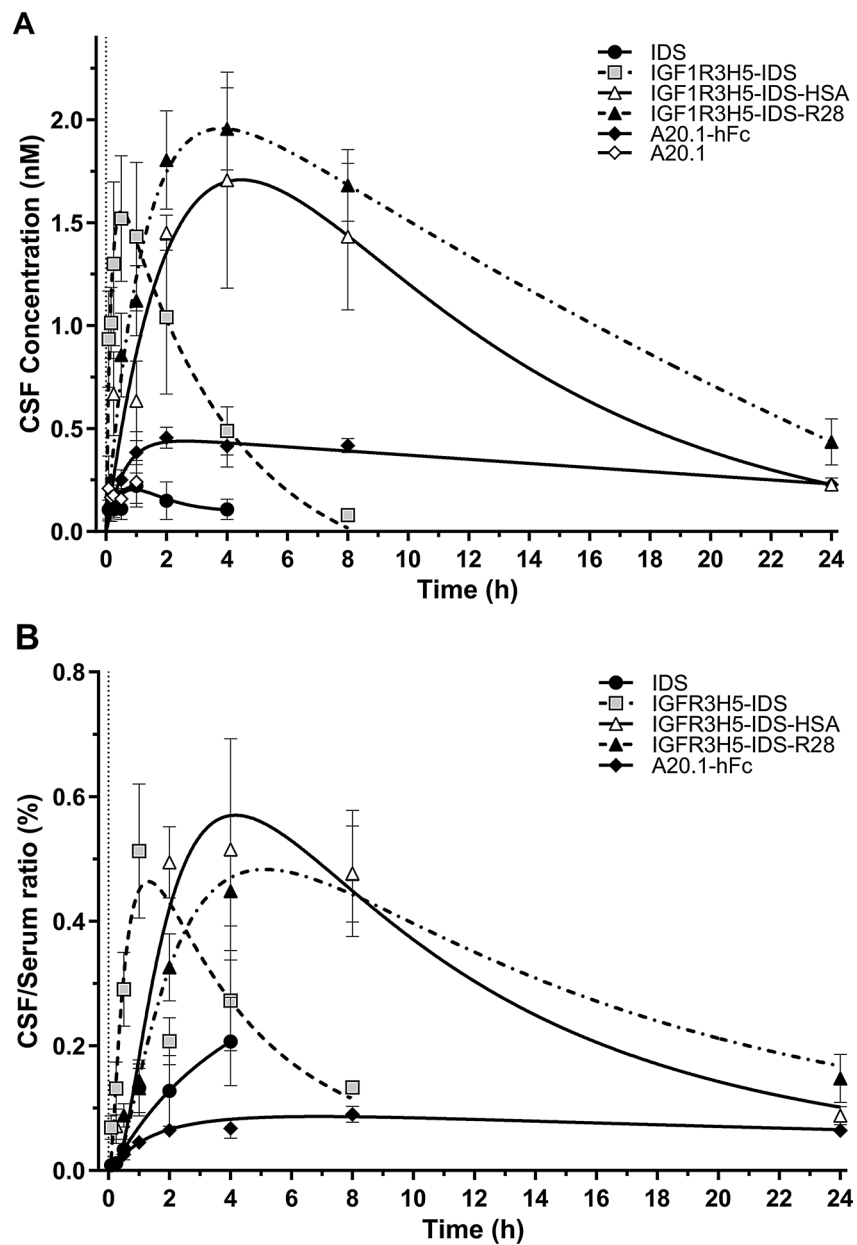


Fig. 3 Brain exposure of IDS is enhanced by fusion with IGF1R3H5 and HSA or anti-serum albumin sdAbs (R28, M79) in rats. **(A)** Marginal levels of A20.1 and IDS were detected in CSF following i.v. administration (76 nmol/kg) for up to 1 and 4 h, respectively. Fusion with IGF1R3H5 dramatically increased peak levels in CSF; further fusion with HSA or R28 prolonged the presence of high levels of IDS in CSF. In contrast, levels of A20.1-hFc remained low despite extended presence in serum. **(B)** Analysis of the CSF/Serum showed that the duration of brain exposure reflects the presence in serum, while peak levels are attributable to the inclusion of a IGF1R3H5. Values represent mean +/- SEM

Table 3 Mean AUC_{last} of the CSF concentration-time profiles and the ratio over AUC_{last} of the serum concentration-time profiles following intravenous bolus administration of A20.1-hFc or IDS constructs to naïve rats

Parameter	Unit	A20.1-hFc	IDS	IGF1R3H5-IDS	IGF1R3H5-IDS-HSA	IGF1R3H5-IDS-R28
$C_{CSF\ max}$	nmol/L	0.42	0.22	1.56	1.75	1.96
$CSF\ AUC_{last}$	nmol*min/mL	0.50	0.03	0.29	1.47	1.82
$Serum\ AUC_{last}$	nmol*min/mL	717.01	51.45	121.07	466.43	914.63
$CSF\ AUC_{last}/Serum\ AUC_{last}$	%	0.07	0.07	0.24	0.32	0.20

$C_{CSF\ max}$: Observed maximum concentration in CSF. AUC_{last} : area under the plasma concentration time curve from time 0 to the last measured time point

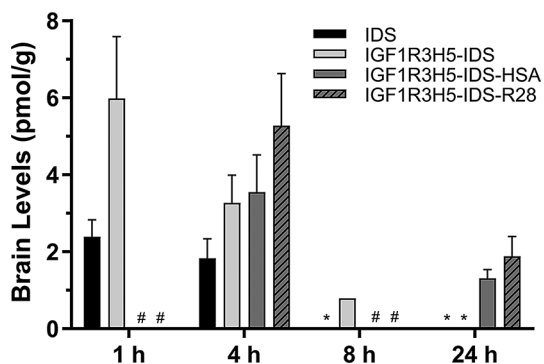


Fig. 4 IDS levels observed in whole brain following i.v. administration (76 nmol/kg) in rats. Low (marginal detection) levels of IDS were present in whole brain for up to 4 h post-administration. Fusion with IGF1R3H5 increased peak levels and duration of detection in whole brain. Addition of the half-life extenders (HSA; anti-serum albumin sdAb, R28) resulted in increased levels at 4 h and extension of detection to 24 h post-administration. * not detected; # not determined

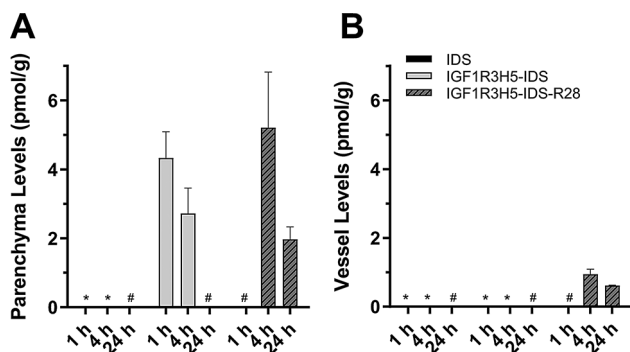


Fig. 5 IDS levels observed in brain and vessels following i.v. administration (76 nmol/kg) in rats. (A-B) Comparison of test article levels over time in brain fractions. IDS was below the detection limits in both brain parenchyma and vessels at all time points. IGF1R3H5-IDS was present in brain parenchyma (A) up to 4 h post-administration and IGF1R3H5-IDS-R28 was present in brain parenchyma and vessels (B) up to 24 h post-administration. * not detected; # not determined

constructs in the vessel component is likely to be limited and that delivery to the parenchyma is achieved. An additional experiment was conducted using higher doses (140 nmol/kg) of the test articles. Supplemental Fig. 5 shows IDS and IGF1R3H5-IDS-HSA concentrations in rat brain parenchyma and vessels. The data confirms that IDS is detectable in whole brain at 1 and 4 h, but not at 24 h. The figure also demonstrates IGF1R3H5-IDS-HSA levels were much greater than IDS and the non-BBB crossing controls (A20.1 VHH and A20.1-hFc). Importantly, IDS and A20.1-hFc were not detectable in brain parenchyma at 4 h (levels at 1 and 24 h were not determined), while IDS is present at marginally detectable levels in brain vessels at 4 h. In stark contrast, the majority of IGF1R3H5-IDS-HSA was found in the brain parenchyma and was not observed to be trapped in brain vessels. Furthermore, the low level of brain vessel “trapping” in the in vivo

studies is consistent with observations in the in vitro BBB models. To further demonstrate the ability of IGF1R3H5 to enable delivery to brain parenchyma, Supplemental Fig. 6 shows the correlations between test article levels in whole brain and brain fractions. The figure shows that the whole brain levels of the BBB impermeable protein A20.1-hFc exhibited weak correlations with the levels in brain fractions. In contrast, IGF1R3H5-IDS-R28 exhibited a strong correlation between levels in brain and parenchyma, but not between brain and vessels.

Discussion

Intravenous ERT has been available for Hunter syndrome for over 10 years, and its ability to alleviate somatic symptoms has been documented in numerous clinical trials [22, 23]. However, standard intravenous delivery was found to be of doubtful benefit to patients with mild cognitive impairment, and of no significant benefit to patients with severe cognitive deterioration [24, 25]. The ineffectiveness of first generation ERT in treating the CNS symptoms of lysosomal storage diseases is attributable to the presence of the BBB, which protects the brain from blood components that would interfere with brain function [26]. As an alternative, intrathecal (IT) infusion is a strategy being developed to address the cognitive symptoms of LSDs [3, 25, 27, 28]. While IT administration was shown to reduce glycosaminoglycan concentrations in the CSF of Hunter syndrome patients [25, 29], it remains to be confirmed if cognitive dysfunction can be successfully alleviated using this strategy [30]. Moreover, it is questionable whether or not administration to the CSF can achieve diffuse intraparenchymal penetration in humans [30]. Similarly, clinically implemented medical procedures such as mannitol-induced osmotic BBB disruption [31] and focused ultrasound [32] have yet to show clinical benefits in treating the brain with biotherapeutics. Therefore, the implementation of non-invasive transvascular brain delivery technologies remain critical for enabling successful therapeutic delivery to the CNS.

Antibodies that bind receptors on brain endothelial cells and subsequently undergo RMT have been developed as a means to enable the brain delivery of protein therapeutics [6]. The delivery of IDS by targeting TfR1 for RMT has been developed [8, 33–39]. While strategies targeting TfR1 have been successful in achieving enhanced brain delivery and therapeutic efficacy, TfR1 is broadly distributed throughout the body and lacks BBB specificity [6]. Similarly, antibodies targeting the insulin receptor have been used to deliver enzymes across the BBB [8, 33–39]. Here we have shown that RMT of IDS through the BBB can be achieved by fusion with a sdAb that targets IGF1R (Fig. 1). Previous studies have shown that anti-IGF1R sdAbs are capable of crossing the in vitro and in vivo BBB, as well as delivering physiologically

relevant therapeutic levels [40, 41]. In contrast to studies involving fusion of anti-IGF1R sdAbs with Fc or therapeutic peptides (such as galanin or neurotensin), the present study showed that fusion with IDS produced a notable reduction in the affinity of the anti-IGF1R sdAbs toward IGF1R and anti-serum albumin sdAbs toward albumin (Table 1). It should be noted that reduced sdAb affinity is not observed in Fc fusion constructs, indicating that this phenomenon is not simply related to the size of the construct, but rather likely due to some level of steric clash preventing unobstructed binding to the SPR surface and possibly to the target antigens *in vivo* [42]. Since it is not clear if the reduced SPR-derived affinity is truly physiological, it cannot be cited as the mechanism for the observed reduction in BBB permeability relative to the parent sdAbs (Fig. 1).

When delivered intravenously, IDS is consistently found to be rapidly cleared from the circulation in rodents ($t_{1/2} < 2$ h) [43, 44], humans and primates ($t_{1/2} < 10$ h) [45, 46]. While serum $t_{1/2}$ is not representative of tissue $t_{1/2}$, which is reported to be 1–2 days for intravenously administered IDS [47], it does present a limitation in delivery to the brain, which has extremely low exposure to serum proteins [6]. This was clearly shown by Garcia et al. [44], who reported that only a minute proportion of the administered dose was found in the brain and is likely present in the microcirculation rather than the brain parenchyma. In the present study, we confirmed that *i.v.* administered IDS was rapidly cleared from the circulation ($t_{1/2\alpha} < 10$ min) in rats, with marginally detectable brain exposure (CSF) and no evidence for the presence of IDS in the brain parenchyma. The rapid clearance of IDS from the blood is the result of uptake by peripheral tissues. It has been reported that >33% of the injected dose is found in the liver 2 h after IDS administration [44].

The mechanism for cellular uptake of therapeutic enzymes lacking RMT functionality relies on endocytosis mediated by the mannose-6-phosphate receptor (M6PR) or the mannose receptor [4, 47–49]. These receptors are broadly distributed throughout the periphery and lack specificity for neuronal populations. As a consequence, a large amount of the injected enzyme is lost before reaching the brain due to a peripheral ‘sink-effect’ that severely reduces the overall efficacy of the treatment [4, 50–52]. The magnitude of this effect was demonstrated in studies using chemical modification of sulfamidase that disrupts glycan structures [52, 53]. Disruption of Man6-P moieties dramatically decreased endocytosis in fibroblasts, and produced a similarly large prolongation of serum concentrations following *i.v.* administration. In our study, we compared the *in vitro* BBB permeability of IDS containing terminal Man-6-P on its glycans (uncapped IDS) with IDS on which the terminal Man-6-P moieties are blocked

for interaction with the M6PR (capped IDS). No difference was observed between the capped and uncapped constructs, indicating that Man-6-P-mediated transcytosis did not contribute to BBB permeability (Fig. 1, unpublished observations).

In an attempt to maximize IDS delivery to the parenchyma, we aimed to determine if serum PK could be extended by constructing fusion proteins containing either human albumin or sdAbs that bind serum albumin. As expected, fusion proteins containing either HSA or anti-serum albumin sdAbs exhibited marked increases in serum PK parameters (Fig. 2; Table 2). The consequence of extended serum PK was a dramatic prolongation of brain exposure (Fig. 3, Suppl. Figure 5). Similarly, we showed that delivery to brain parenchyma correlated well with brain exposure and that therapeutically relevant amounts of IDS were present for up to 24 h following a single administration (Fig. 4). Moreover, we were able to confirm that the observed increases in IDS levels within the brain were not due to uptake and retention by the vascular bed (Suppl. Figure 6).

Conclusions

The study presented here further demonstrates the viability of BBB-permeable IDS-sdAb fusion proteins with extended serum $t_{1/2}$ as a potential therapeutic for Hunter syndrome. This is the first demonstration of an LSD therapeutic with extended serum $t_{1/2}$ that does not require a full Fc domain. The strategy described herein represents a versatile platform technology that is amenable to bio-manufacturing and can be redeployed for the numerous other LSDs with CNS pathology.

Abbreviations

ABC	Ammonium bicarbonate
AUC	Under the curve
BBB	Blood-brain barrier
CNS	Central nervous system
CSF	Cerebrospinal fluid
DOC	Sodium deoxycholate
DTT	dl-dithiothreitol
ERT	Enzyme replacement therapy
FBS	Fetal bovine serum
HBSS	Hanks’ balanced salt solution
hFc	Human Fc
HAS	Human serum albumin
iBEC	iPSC-derived brain endothelial cell
IDS	Iduronate-2-sulfatase
IGF1R	Insulin-like growth factor 1 receptor
IMAC	Immobilized metal-affinity chromatography
iPSC	Induced pluripotent stem cell
IT	Intrathecal
JBMan	Jack bean α -mannosidase
LSD	Lysosomal storage disease
Man-6-P	Mannose-6-phosphate
MPS II	Mucopolysaccharidosis type II
P_{APP}	Apparent permeability
PK	Pharmacokinetics
RA	Retinoic acid
RMT	Receptor-mediated transcytosis
sdAb	Single-domain antibody

SFTB	Sulfate-free transport buffer
SPR	Surface plasmon resonance
SRM	Selected reaction monitoring
TB	Transport buffer
TEER	Transendothelial electrical resistance
TfR	Transferrin receptor
TMEM30A	Transmembrane protein 30 A
VHH	Variable heavy domain of heavy chain camelid antibody

Supplementary Information

The online version contains supplementary material available at <https://doi.org/10.1186/s12987-024-00617-6>.

Supplementary Material 1

Acknowledgements

The authors thank members of the In Vitro Pharmacology, Single Domain Antibodies and Bioanalysis Teams (NRC) for their technical contributions. This manuscript is dedicated to the loving memory of Dr. Danica Stanimirovic, whose leadership and pioneering work on the blood brain barrier has been an inspiration for us all.

Author contributions

W.J.C.: Contributed to the planning and execution of the experiments, conducted data and statistical analysis, prepared the figures and drafted/wrote and reviewed the manuscript. Corresponding author. A.S.H.: Supervised the quantitative proteomics studies, performed data analysis and contributed to writing/reviewing the manuscript. G.H.: Created the anti-albumin antibodies, conducted the SPR analysis and contributed to writing/reviewing the manuscript. H.v.F.: Conducted the SPR experiments. E.L., B.L.: Performed the PK analyses and contributed to writing/reviewing the manuscript. E.B, D.L.: Performed experiments and project co-ordination. H.F.: Contributed to the initial project conceptualization and planning. J.B., S.G, G.P, K.P., S.R., F.F.: Designed, produced and characterized all of the protein constructs used and contributed to writing/reviewing the manuscript. W.V.: Contributed to the conceptualization of the study and to writing/reviewing the manuscript. D.S.: Created the BBB-Trojan antibodies, contributed to the conceptualization of the study and to writing/reviewing the manuscript.

Funding

Funding for this project was provided by Oxyrane.

Data availability

No datasets were generated or analysed during the current study.

Declarations

Ethical approval

All animal experiments were conducted at the National Research Council and prior ethical approval for the studies was obtained from the NRC Animal Care Committee. The NRC maintains active certification by the Canadian Council on Animal Care (CCAC) and conforms to their guidelines pertaining to research ethics involving rats. All studies described herein comply with the ARRIVE guidelines.

Competing interests

The authors declare no competing interests.

Received: 6 November 2024 / Accepted: 23 December 2024

Published online: 14 January 2025

References

- Parenti G, Andria G, Ballabio A. Lysosomal storage diseases: from pathophysiology to therapy. *Annu Rev Med* [Internet]. 2015;66:471–86. Available from: <http://www.ncbi.nlm.nih.gov/pubmed/25587658>
- Begley D, Pontikis C, Scarpa M. Lysosomal Storage Diseases and the Blood-Brain Barrier. *Curr Pharm Des* [Internet]. 2008;14:1566–80. Available from: <http://www.eurekaselect.com/openurl/content.php?genre=article&issn=1381-6128&volume=14&issue=16&page=1566>
- Edelmann MJ, Maegawa GHB. CNS-Targeting Therapies for Lysosomal Storage Diseases: Current Advances and Challenges. *Front Mol Biosci* [Internet]. 2020;7:559804. Available from: <http://www.ncbi.nlm.nih.gov/pubmed/33304924>
- Sands MS, Vogler CA, Ohlemiller KK, Roberts MS, Grubb JH, Levy B et al. Biodistribution, kinetics, and efficacy of highly phosphorylated and non-phosphorylated beta-glucuronidase in the murine model of mucopolysaccharidosis VII. *J Biol Chem* [Internet]. 2001;276:43160–5. Available from: <http://www.ncbi.nlm.nih.gov/pubmed/11562370>
- Abbott NJ, Patabendige AAK, Dolman DEM, Yusof SR, Begley DJ. Structure and function of the blood-brain barrier. *Neurobiol Dis* [Internet]. 2010;37:13–25. Available from: <http://www.ncbi.nlm.nih.gov/pubmed/19664713>
- Stanimirovic DB, Sandhu JK, Costain WJ. Emerging Technologies for Delivery of Biotherapeutics and Gene Therapy Across the Blood-Brain Barrier. *BioDrugs* [Internet]. 2018;32:547–59. Available from: <http://link.springer.com/https://doi.org/10.1007/s40259-018-0309-y>
- Okuyama T, Eto Y, Sakai N, Nakamura K, Yamamoto T, Yamaoka M et al. A Phase 2/3 Trial of Pabinafusp Alfa, IDS Fused with Anti-Human Transferrin Receptor Antibody, Targeting Neurodegeneration in MPS-II. *Mol Ther* [Internet]. 2020; Available from: <http://www.ncbi.nlm.nih.gov/pubmed/33038326>
- Ullman JC, Arguello A, Getz JA, Bhalla A, Mahon CS, Wang J et al. Brain delivery and activity of a lysosomal enzyme using a blood-brain barrier transport vehicle in mice. *Sci Transl Med* [Internet]. 2020;12. Available from: <http://www.ncbi.nlm.nih.gov/pubmed/32461331>
- Webster CI, Caram-Salas N, Haqqani AS, Thom G, Brown L, Rennie K et al. Brain penetration, target engagement, and disposition of the blood-brain barrier-crossing bispecific antibody antagonist of metabotropic glutamate receptor type 1. *FASEB J* [Internet]. 2016 [cited 2016 Feb 4];30:1927–40. Available from: <http://www.ncbi.nlm.nih.gov/pubmed/26839377>
- Muruganandam A, Tanha J, Narang S, Stanimirovic D. Selection of phage-displayed llama single-domain antibodies that transmute across human blood-brain barrier endothelium. *FASEB J* [Internet]. 2002;16:240–2. Available from: <http://www.ncbi.nlm.nih.gov/pubmed/11772942>
- Stanimirovic DB, Kemmerich K, Haqqani AS, Sulea T, Arbabi-Ghahroudi M, Massie B, et al. Insulin-like growth factor 1 receptor -specific antibodies and uses thereof. *United States: USPTO*; 2017. p. 42.
- Abulrob A, Sprong H, Van Bergen P, Stanimirovic D. The blood-brain barrier transmuting single domain antibody: mechanisms of transport and antigenic epitopes in human brain endothelial cells. *J Neurochem* [Internet]. 2005;95:1201–14. Available from: <https://doi.org/10.1111/j.1471-4159.2005.03463.x>
- Sheff J, Wang P, Xu P, Arbour M, Masson L, van Faassen H et al. Defining the epitope of a blood-brain barrier crossing single domain antibody specific for the type 1 insulin-like growth factor receptor. *Sci Rep* [Internet]. 2021;11:4284. Available from: <http://www.ncbi.nlm.nih.gov/pubmed/33608571>
- Henry KA, Tanha J, Hussack G. Identification of cross-reactive single-domain antibodies against serum albumin using next-generation DNA sequencing. *Protein Eng Des Sel* [Internet]. 2015 [cited 2016 Oct 24];28:379–83. Available from: <http://www.ncbi.nlm.nih.gov/pubmed/26319004>
- van Faassen H, Ryan S, Henry KA, Raphael S, Yang Q, Rossotti MA et al. Serum albumin-binding VHHs with variable pH sensitivities enable tailored half-life extension of biologics. *FASEB J* [Internet]. 2020;34:8155–71. Available from: <http://www.ncbi.nlm.nih.gov/pubmed/32342547>
- Tanha J, Muruganandam A, Stanimirovic D. Phage display technology for identifying specific antigens on brain endothelial cells. *Methods Mol Med* [Internet]. 2003;89:435–49. Available from: <http://www.ncbi.nlm.nih.gov/pubmed/12958438>
- Bélangier K, Iqbal U, Tanha J, MacKenzie R, Moreno M, Stanimirovic D. Single-Domain Antibodies as Therapeutic and Imaging Agents for the Treatment of CNS Diseases. *Antibodies (Basel, Switzerland)* [Internet]. 2019;8. Available from: <http://www.ncbi.nlm.nih.gov/pubmed/31544833>
- Sodja C, Callaghan D, Haqqani AS, Stanimirovic DB, Costain WJ, Jezierski A. Immunoassay for Quantitative Detection of Antibody Transcytosis Across the Blood-Brain Barrier In Vitro. *Methods Mol Biol* [Internet]. 2022;2549:345–57. Available from: <http://www.ncbi.nlm.nih.gov/pubmed/35218529>
- Ribocco-Lutkiewicz M, Sodja C, Haukenfrers J, Haqqani AS, Ly D, Zachar P et al. A novel human induced pluripotent stem cell blood-brain barrier model: Applicability to study antibody-triggered receptor-mediated transcytosis. *Sci Rep* [Internet]. 2018;8:1873. Available from: <http://www.ncbi.nlm.nih.gov/pubmed/29382846>

20. Ying T, Chen W, Gong R, Feng Y, Dimitrov DS. Soluble monomeric IgG1 Fc. *J Biol Chem* [Internet]. 2012;287:19399–408. Available from: <http://www.jbc.org/lookup/doi/https://doi.org/10.1074/jbc.M112.368647>
21. Stojanovic F, Taktek M, Khieu NH, Huang J, Jiang S, Rennie K et al. NMR analysis of the correlation of metabolic changes in blood and cerebrospinal fluid in Alzheimer model male and female mice. Ginsberg SD, editor. *PLoS One* [Internet]. 2021;16:e0250568. Available from: <https://doi.org/10.1371/journal.pone.0250568>
22. Wikman-Jorgensen PE, López Amorós A, Peris García J, Esteve Atienzar PJ, Cañizares Navarro R, Asensio Tomás ML et al. Enzyme replacement therapy for the treatment of Hunter disease: A systematic review with narrative synthesis and meta-analysis. *Mol Genet Metab* [Internet]. 2020;131:206–10. Available from: <http://www.ncbi.nlm.nih.gov/pubmed/32773276>
23. Muenzer J, Botha J, Harmatz P, Giugliani R, Kampmann C, Burton BK. Evaluation of the long-term treatment effects of intravenous idursulfase in patients with mucopolysaccharidosis II (MPS II) using statistical modeling: data from the Hunter Outcome Survey (HOS). *Orphanet J Rare Dis* [Internet]. 2021;16:456. Available from: <http://www.ncbi.nlm.nih.gov/pubmed/34717704>
24. Muenzer J, Bodamer O, Burton B, Clarke L, Frenking GS, Giugliani R et al. The role of enzyme replacement therapy in severe Hunter syndrome-an expert panel consensus. *Eur J Pediatr* [Internet]. 2012 [cited 2016 Feb 13];171:181–8. Available from: <http://www.pubmedcentral.nih.gov/articlerender.fcgi?artid=3249184&tool=pmcentrez&rendertype=abstract>
25. Muenzer J, Hendriks CJ, Fan Z, Vijayaraghavan S, Perry V, Santra S et al. A phase I/II study of intrathecal idursulfase-IT in children with severe mucopolysaccharidosis II. *Genet Med* [Internet]. 2016 [cited 2016 Feb 13];18:73–81. Available from: <http://www.ncbi.nlm.nih.gov/pubmed/25834948>
26. Daneman R, Prat A. The blood-brain barrier. *Cold Spring Harb Perspect Biol* [Internet]. 2015;7:a020412. Available from: <http://www.ncbi.nlm.nih.gov/pubmed/25561720>
27. Terstappen GC, Meyer AH, Bell RD, Zhang W. Strategies for delivering therapeutics across the blood-brain barrier. *Nat Rev Drug Discov* [Internet]. 2021;20:362–83. Available from: <http://www.ncbi.nlm.nih.gov/pubmed/33649582>
28. Muenzer J, Hendriks CJ, Stein MB, Fan Z, Kearney S, Horton J et al. A long-term extension study evaluating intrathecal idursulfase-IT in children with Hunter syndrome and cognitive impairment. *Mol Genet Metab* [Internet]. 2017;120:599–100. Available from: <https://linkinghub.elsevier.com/retrieve/pii/S1096719216306680>
29. Muenzer J, Vijayaraghavan S, Stein M, Kearney S, Wu Y, Alexanderian D. Long-term open-label phase I/II extension study of intrathecal idursulfase-IT in the treatment of neuronopathic mucopolysaccharidosis II. *Genet Med* [Internet]. 2022; Available from: <http://www.ncbi.nlm.nih.gov/pubmed/35588317>
30. Sato Y, Minami K, Hirato T, Tanizawa K, Sonoda H, Schmidt M. Drug delivery for neuronopathic lysosomal storage diseases: evolving roles of the blood brain barrier and cerebrospinal fluid. *Metab Brain Dis* [Internet]. 2022; Available from: <http://www.ncbi.nlm.nih.gov/pubmed/35088290>
31. Bellavance M-A, Blanchette M, Fortin D. Recent advances in blood-brain barrier disruption as a CNS delivery strategy. *AAPS J* [Internet]. 2008;10:166–77. Available from: <http://www.ncbi.nlm.nih.gov/pubmed/18446517>
32. Poon C, McMahon D, Hynynen K. Noninvasive and targeted delivery of therapeutics to the brain using focused ultrasound. *Neuropharmacology* [Internet]. 2017;120:20–37. Available from: <http://www.ncbi.nlm.nih.gov/pubmed/26907805>
33. Boado RJ, Zhang YYY, Zhang YYY, Xia C-F, Wang Y, Pardridge WM. Genetic engineering of a lysosomal enzyme fusion protein for targeted delivery across the human blood-brain barrier. *Biotechnol Bioeng* [Internet]. 2008 [cited 2016 Feb 18];99:475–84. Available from: <http://www.ncbi.nlm.nih.gov/pubmed/17680664>
34. Boado RJ, Hui EK-W, Lu JZ, Zhou Q-H, Pardridge WM. Reversal of lysosomal storage in brain of adult MPS-I mice with intravenous Trojan horse-iduronidase fusion protein. *Mol Pharm* [Internet]. 2011 [cited 2016 Feb 18];8:1342–50. Available from: <http://www.ncbi.nlm.nih.gov/pubmed/21667973>
35. Boado RJ, Hui EK-W, Lu JZ, Sumbria RK, Pardridge WM. Blood-brain barrier molecular trojan horse enables imaging of brain uptake of radioiodinated recombinant protein in the rhesus monkey. *Bioconjug Chem* [Internet]. 2013 [cited 2016 Jan 31];24:1741–9. Available from: <http://www.ncbi.nlm.nih.gov/pubmed/24059813>
36. Zhou Q-H, Boado RJ, Lu JZ, Hui EK-W, Pardridge WM. Brain-penetrating IgG-iduronate 2-sulfatase fusion protein for the mouse. *Drug Metab Dispos* [Internet]. 2012;40:329–35. Available from: <http://www.ncbi.nlm.nih.gov/pubmed/22065691>
37. Giugliani R, Martins AM, Okuyama T, Eto Y, Sakai N, Nakamura K et al. Enzyme Replacement Therapy with Pabinafusp Alfa for Neuronopathic Mucopolysaccharidosis II: An Integrated Analysis of Preclinical and Clinical Data. *Int J Mol Sci* [Internet]. 2021;22. Available from: <http://www.ncbi.nlm.nih.gov/pubmed/34681597>
38. Yamamoto R, Yoden E, Tanaka N, Kinoshita M, Imakiire A, Hirato T et al. Nonclinical safety evaluation of pabinafusp alfa, an anti-human transferrin receptor antibody and iduronate-2-sulfatase fusion protein, for the treatment of neuronopathic mucopolysaccharidosis type II. *Mol Genet Metab Reports* [Internet]. 2021;27:100758. Available from: <https://linkinghub.elsevier.com/retrieve/pii/S2214426921000525>
39. Tomita K, Okamoto S, Seto T, Hamazaki T, So S, Yamamoto T et al. Divergent developmental trajectories in two siblings with neuropathic mucopolysaccharidosis type II (Hunter syndrome) receiving conventional and novel enzyme replacement therapies: A case report. *JIMD Rep* [Internet]. 2021;62:9–14. Available from: <http://www.ncbi.nlm.nih.gov/pubmed/34765392>
40. Alata W, Yogi A, Brunette E, Delaney CE, van Faassen H, Hussack G et al. Targeting insulin-like growth factor-1 receptor (IGF1R) for brain delivery of biologics. *FASEB J* [Internet]. 2022;36:e22208. Available from: <http://www.ncbi.nlm.nih.gov/pubmed/35192204>
41. Yogi A, Hussack G, van Faassen H, Haqqani AS, Delaney CE, Brunette E et al. Brain Delivery of IGF1R5, a Single-Domain Antibody Targeting Insulin-like Growth Factor-1 Receptor. *Pharmaceutics* [Internet]. 2022;14. Available from: <http://www.ncbi.nlm.nih.gov/pubmed/35890347>
42. Schuck P, Zhao H. The role of mass transport limitation and surface heterogeneity in the biophysical characterization of macromolecular binding processes by SPR biosensing. *Methods Mol Biol* [Internet]. 2010;627:15–54. Available from: <http://www.ncbi.nlm.nih.gov/pubmed/20217612>
43. Boado RJ, Ka-Wai Hui E, Zhiqiang Lu J, Pardridge WM. Insulin receptor antibody-iduronate 2-sulfatase fusion protein: pharmacokinetics, anti-drug antibody, and safety pharmacology in Rhesus monkeys. *Biotechnol Bioeng* [Internet]. 2014 [cited 2016 Feb 18];111:2317–25. Available from: <http://www.pubmedcentral.nih.gov/articlerender.fcgi?artid=4176522&tool=pmcentrez&rendertype=abstract>
44. Garcia AR, DaCosta JM, Pan J, Muenzer J, Lamsa JC. Preclinical dose ranging studies for enzyme replacement therapy with idursulfase in a knock-out mouse model of MPS II. *Mol Genet Metab* [Internet]. 2007;91:183–90. Available from: <http://www.ncbi.nlm.nih.gov/pubmed/17459751>
45. Sohn YB, Cho SY, Park SW, Kim SJ, Ko A-R, Kwon E-K et al. Phase I/II clinical trial of enzyme replacement therapy with idursulfase beta in patients with mucopolysaccharidosis II (Hunter Syndrome). *Orphanet J Rare Dis* [Internet]. *BioMed Central*; 2013 [cited 2017 Nov 21];8:42. Available from: <http://ojrd.bio-medcentral.com/articles/https://doi.org/10.1186/1750-1172-8-42>
46. Xie H, Chung J-K, Mascelli MA, McCauley TG. Pharmacokinetics and bioavailability of a therapeutic enzyme (idursulfase) in cynomolgus monkeys after intrathecal and intravenous administration. *PLoS One* [Internet]. 2015;10:e0122453. Available from: <http://www.ncbi.nlm.nih.gov/pubmed/25836678>
47. Whiteman DA, Kimura A. Development of idursulfase therapy for mucopolysaccharidosis type II (Hunter syndrome): the past, the present and the future. *Drug Des Devel Ther* [Internet]. 2017;11:2467–80. Available from: <http://www.ncbi.nlm.nih.gov/pubmed/28860717>
48. Shen J-S, Busch A, Day TS, Meng X-L, Yu Ci, Dabrowska-Schlepp P et al. Mannose receptor-mediated delivery of moss-made α -galactosidase A efficiently corrects enzyme deficiency in Fabry mice. *J Inher Metab Dis* [Internet]. 2016;39:293–303. Available from: <http://www.ncbi.nlm.nih.gov/pubmed/26310963>
49. Muenzer J, Gucsavas-Calikoglu M, McCandless SE, Schuetz TJ, Kimura A. A phase I/II clinical trial of enzyme replacement therapy in mucopolysaccharidosis II (Hunter syndrome). *Mol Genet Metab* [Internet]. 2007 [cited 2016 Feb 29];90:329–37. Available from: <http://www.ncbi.nlm.nih.gov/pubmed/17185020>
50. Fang H, Stanimirovic D, Haqqani A, Costain W, Hussack G. Blood-Brain Barrier Transmigrating Therapeutic Compounds and Uses Thereof [Internet]. Canada; 2019. Available from: https://www.ic.gc.ca/opic-cipo/cpd/eng/patent/3098162/summary.html?type=number_search&tabs1Index=tabs1_1#tabs1_1
51. Cadaoas J, Boyle G, Jungles S, Cullen S, Vellard M, Grubb JH et al. Vestronidase alfa: Recombinant human β -glucuronidase as an enzyme replacement

- therapy for MPS VII. *Mol Genet Metab* [Internet]. 2020;130:65–76. Available from: <http://www.ncbi.nlm.nih.gov/pubmed/32192868>
52. Gustavsson S, Ohlin Sjöström E, Tjernberg A, Janson J, Westermarck U, Andersson T et al. Intravenous delivery of a chemically modified sulfamidase efficiently reduces heparan sulfate storage and brain pathology in mucopolysaccharidosis IIIA mice. *Mol Genet Metab reports* [Internet]. 2019;21:100510. Available from: <https://www.ncbi.nlm.nih.gov/pubmed/31528541>
 53. Janson J, Andersson G, Bergquist L, Eriksson M, Folgering JHA. Impact of chemical modification of sulfamidase on distribution to brain interstitial fluid and to CSF after an intravenous administration in awake, freely-moving rats. *Mol Genet Metab reports* [Internet]. 2020;22:100554. Available from: <http://www.ncbi.nlm.nih.gov/pubmed/31908953>
 54. Vervecken W, Ryckaert S, Valesvska AV. Production of catalytically active type i sulfatase [Internet]. GB: World Intellectual Property Organization; 2014. p. 129. Available from: <https://patents.google.com/patent/WO2014136065A2/en?q=WO2014136065A2>
 55. Tiels P, Baranova E, Piens K, De Visscher C, Pynaert G, Nerinckx W et al. A bacterial glycosidase enables mannose-6-phosphate modification and improved cellular uptake of yeast-produced recombinant human lysosomal enzymes. *Nat Biotechnol* [Internet]. 2012;30:1225–31. Available from: <http://www.ncbi.nlm.nih.gov/pubmed/23159880>
 56. De Pourcq K, Vervecken W, Dewerte I, Valevska A, Van Hecke A, Callewaert N. Engineering the yeast *Yarrowia lipolytica* for the production of therapeutic proteins homogeneously glycosylated with Man₈GlcNAc₂ and Man₂GlcNAc₂. *Microb Cell Fact* [Internet]. 2012;11:53. Available from: <http://www.ncbi.nlm.nih.gov/pubmed/22548968>
 57. Garberg P, Ball M, Borg N, Cecchelli R, Fenart L, Hurst RD et al. In vitro models for the blood-brain barrier. *Toxicol In Vitro* [Internet]. 2005 [cited 2016 Mar 3];19:299–334. Available from: <http://www.ncbi.nlm.nih.gov/pubmed/15713540>
 58. Haqqani AS, Caram-Salas N, Ding W, Brunette E, Delaney CE, Baumann E et al. Multiplexed evaluation of serum and CSF pharmacokinetics of brain-targeting single-domain antibodies using a NanoLC-SRM-ILIS method. *Mol Pharm* [Internet]. 2013 [cited 2016 Mar 10];10:1542–56. Available from: <http://www.ncbi.nlm.nih.gov/pubmed/23150993>
 59. Artursson P, Karlsson J. Correlation between oral drug absorption in humans and apparent drug permeability coefficients in human intestinal epithelial (Caco-2) cells. *Biochem Biophys Res Commun* [Internet]. 1991 [cited 2016 Mar 30];175:880–5. Available from: <http://www.ncbi.nlm.nih.gov/pubmed/1673839>
 60. Nirogi R, Kandikere V, Mudigonda K, Bhyrapuneni G, Muddana N, Saralaya R et al. A simple and rapid method to collect the cerebrospinal fluid of rats and its application for the assessment of drug penetration into the central nervous system. *J Neurosci Methods* [Internet]. 2009 [cited 2016 Mar 29];178:116–9. Available from: <http://www.ncbi.nlm.nih.gov/pubmed/19109998>
 61. Fluttert M, Dalm S, Oitzl MS. A refined method for sequential blood sampling by tail incision in rats. *Lab Anim* [Internet]. 2000 [cited 2016 Mar 10];34:372–8. Available from: <http://www.ncbi.nlm.nih.gov/pubmed/11072857>
 62. Haqqani AS, Kelly JF, Stanimirovic DB. Quantitative protein profiling by mass spectrometry using isotope-coded affinity tags. *Methods Mol Biol* [Internet]. 2008/03/29. 2008;439:225–40. Available from: http://www.ncbi.nlm.nih.gov/entrez/query.fcgi?cmd=Retrieve&db=PubMed&dopt=Citation&list_uids=18370107

Publisher's note

Springer Nature remains neutral with regard to jurisdictional claims in published maps and institutional affiliations.